



## RESEARCH LETTER

10.1002/2017GL072678

## Key Points:

- PFISR-observed ionospheric plasma responses to field-aligned currents and ionospheric convection vortices formed during sudden commencement
- Responses include *F* region plasma lifting, field-aligned ion upflow, density decrease, short-lived  $T_i$  increase and long-lasting  $T_e$  increase
- Global MHD simulation reproduced the magnetic perturbation on the ground and revealed SC-related FACs and convection evolutions

## Supporting Information:

- Supporting Information S1

## Correspondence to:

S. Zou,  
shashaz@umich.edu

## Citation:

Zou, S., D. Ozturk, R. Varney, and A. Reimer (2017), Effects of sudden commencement on the ionosphere: PFISR observations and global MHD simulation, *Geophys. Res. Lett.*, *44*, 3047–3058, doi:10.1002/2017GL072678.

Received 17 JAN 2017

Accepted 27 MAR 2017

Accepted article online 29 MAR 2017

Published online 14 APR 2017

## Effects of sudden commencement on the ionosphere: PFISR observations and global MHD simulation

Shasha Zou<sup>1</sup> , Dogacan Ozturk<sup>1</sup>, Roger Varney<sup>2</sup> , and Ashton Reimer<sup>2</sup> 

<sup>1</sup>Department of Climate and Space Sciences and Engineering, University of Michigan, Ann Arbor, Michigan, USA, <sup>2</sup>Center for Geospace Studies, SRI International, Menlo Park, California, USA

**Abstract** Sudden commencement (SC) induced by solar wind pressure enhancement can produce significant global impact on the coupled magnetosphere-ionosphere (MI) system, and its effects have been studied extensively using ground magnetometers and coherent scatter radars. However, very limited observations have been reported about the effects of SC on the ionospheric plasma. Here we report detailed Poker Flat Incoherent Scatter Radar (PFISR) observations of the ionospheric response to SC during the 17 March 2015 storm. PFISR observed lifting of the *F* region ionosphere, transient field-aligned ion upflow, prompt but short-lived ion temperature increase, subsequent *F* region density decrease, and persistent electron temperature increase. A global magnetohydrodynamic (MHD) simulation has been carried out to characterize the SC-induced current, convection, and magnetic perturbations. Simulated magnetic perturbations at Poker Flat show a satisfactory agreement with observations. The simulation provides a global context for linking localized PFISR observations to large-scale dynamic processes in the MI system.

### 1. Introduction

A sudden increase of solar wind dynamic pressure associated with an interplanetary shock or a discontinuity leads to a large-scale compression of the magnetosphere, and such a compression is referred to as sudden commencement (SC) based on the ground-based magnetometer observations. SC is usually used to describe a broad range of phenomena, including sudden storm commencement (SSC) and sudden impulse (SI) (see review by *Curto et al.* [2007, and references therein], and emphasizes the compression effect associated with dynamic pressure enhancement regardless of whether or not a geomagnetic storm follows the compression. The effects of sudden commencement on the coupled magnetosphere-ionosphere system have been studied extensively by using ground-based magnetometers and Super Dual Auroral Radar Network (SuperDARN) coherent radars [e.g., *Nishida and Jacobs*, 1962; *Araki*, 1977, 1994; *Kikuchi et al.*, 2001; *Shi et al.*, 2014; *Tian et al.*, 2016]. Depending on the polarities of the magnetic field perturbation and the field-aligned currents (FACs), the response of the coupled system can be characterized into two phases, i.e., the preliminary impulse (PI) phase and the main impulse (MI) phase [*Araki*, 1994]. In general, during the PI phase, the field-aligned currents (FACs) are downward/upward in the afternoon/morning sector and the associated Hall currents inferred from ground-based magnetometers form a counterclockwise/clockwise vortex. During the MI phase, the polarities of the FACs, the direction of the Hall currents and the convection flows reverse.

The formation mechanisms of the PI and MI phases caused by the solar wind dynamic pressure enhancement have been investigated through theoretical studies [e.g., *Kivelson and Southwood*, 1991; *Araki*, 1994] and numerical modeling, mainly global magnetohydrodynamic (MHD) simulations [e.g., *Slinker et al.*, 1999; *Fujita et al.*, 2003a, 2003b, 2005; *Chi et al.*, 2006; *Samsonov et al.*, 2010; *Yu and Ridley*, 2011; *Sun et al.*, 2015; *Kubota et al.*, 2015; *Tian et al.*, 2016]. In these studies, the solar wind dynamic pressure front has been assumed to be of large scale and approach the magnetosphere as a planar discontinuity. Smaller-scale magnetic disturbances sometimes occur on the dayside high-latitude magnetosphere, and they are often called magnetic impulse event [*Lanzerotti et al.*, 1991; *Sibeck and Korotova*, 1996], which are associated with smaller-scale ionospheric convection vortices (traveling convection vortices, or TCVs) and FACs systems [*Friis-Christensen et al.*, 1988; *Glassmeier et al.*, 1989]. These smaller-scale features are suggested to arise from localized solar wind dynamic pressure enhancement or dynamic processes in the foreshock region [e.g., *Moretto et al.*, 1997; *Zesta et al.*, 1999; *Zesta*, 2002; *Murr et al.*, 2002; *Sibeck et al.*, 2003; *Murr and Hughes*, 2003; *Kataoka et al.*, 2003]. *Kataoka et al.* [2003] simulated the FACs systems associated with TCVs by

introducing a localized density perturbation and found that the FACs produced have the same polarities as those induced by large-scale solar wind dynamic pressure enhancement but with much smaller-scale sizes.

Despite numerous studies on the effects of SC on the coupled geospace system, there have been only very limited studies on the effects of SC and the associated transient FACs and convection flows on the ionospheric plasma. *Doupnik et al.* [1977] used Chatanika incoherent scatter radar (ISR) and magnetometers in Alaska to study the ionosphere response to three SCs within 1 day and founded that enhanced ionospheric convection flows occurred during two of the three SC events. Using the European Incoherent Scatter radar and magnetometers, *Collis and Häggström* [1991] performed a case study of the ionospheric plasma response to SC. They observed *F* region electron density depletion, ion temperature increase, and increased horizontal convection flow, but no field-aligned ion upflow event was observed in their case study. These two pioneer works showed the possible effects of SC on ionospheric plasma but could not connect the localized ISR observations with either solar wind measurements or large-scale magnetospheric drivers. *Schunk et al.* [1994] modeled the ionospheric response to a pair of FACs and ionospheric vortices with spatial scales similar to TCVs using the Utah State University time-dependent ionospheric model. Their simulation results revealed localized plasma temperature enhancements, in particular ion temperature, ion composition changes, non-Maxwellian ion distributions, and plasma upwelling.

The terrestrial ionosphere supplies plasma to the magnetosphere through the ion outflow process, in particular, the heavy ions such as  $O^+$ . The  $O^+$  ions play an important role in regulating the dynamics in the magnetosphere, such as changing the ion composition in the ring current and thus its life time, affecting the reconnection rate both on the dayside magnetopause and in the nightside magnetotail [e.g., *Chappell*, 2015; *Lotko*, 2007, and references therein; *Yau et al.*, 2007, and references therein]. *Strangeway et al.* [2005] suggested that ion outflow usually occurs as a two-step process with ion upflow caused by increased ion (so-called Type 1 upflow) and/or increased electron (so-called Type 2 upflow) temperatures in the *F* region and topside ionosphere as the first step. Recently, enhanced *F* region and topside ionosphere density within the storm-enhanced density (SED) region [*Foster et al.*, 2005; *Zou et al.*, 2013, 2014] has been suggested to be a third mechanism of contributing large ion upflow fluxes [*Semeter et al.*, 2003; *Yuan et al.*, 2008; *Zou et al.*, 2017]. The first two mechanisms described above arise from plasma temperature increase, while the third one associated with SED is due to increased plasma source population. Ion upflow pumps the ionospheric plasmas to higher altitudes where they can be further accelerated to velocities exceeding the escape velocity. It has also been suggested that the initial ion upflow flux in the *F* region and topside ionosphere can regulate the total flux of ion outflow [*Nilsson et al.*, 2008]. Therefore, understanding the generation mechanisms of the initial ion upflow under various interplanetary and geomagnetic conditions is of great importance for understanding the ion outflow processes. Field-aligned ion upflows have been observed by ground-based ISRs in the dayside cusp region, in regions of fast ionospheric flows, as well as in regions of strong ionospheric flow shears [*Lühr et al.*, 1993; *Moén et al.*, 2004; *Liu and Lu*, 2004; *Zhang et al.*, 2017]. Statistical studies have shown that the ion upflow fluxes increase with increasing solar wind density and velocity [*Ogawa et al.*, 2009]. However, there are only very limited studies devoted to identifying the physical processes that generate the ion upflow associated with solar wind pressure enhancement.

Ground-based coherent scatter radar requires field-aligned density irregularities in the *F* region in order to scatter the radar signals back. There have been a few studies on the effects of the SC on the radar performance [*Kataoka et al.*, 2003; *Kane and Makarevich*, 2010; *Gillies et al.*, 2012]. *Kataoka et al.* [2003] found enhanced *F* region irregularities excited due to local and strong *F* region density gradient within the convection flow vortex. Using a superposed-epoch analysis, *Gillies et al.* [2012] found that ionospheric plasma drift and radar echoes both increase on the dayside due to the dynamic pressure increase, while the coherent radar irregularities decrease on the nightside despite that the flow speed continues to increase. Therefore, understanding the response of the ionospheric plasma to solar wind dynamic pressure enhancement can help improve the understanding of the related field-aligned irregularities and advance the forecast capability of coherent radar coverage.

Instrument limitation is part of the reason why the ionospheric response to solar wind dynamic pressure enhancement has not been studied extensively. Multiparameter vertical profiles of the ionospheric plasma can only be provided by ground-based ISR. Traditional ISRs need to mechanically shift the antenna steering direction; thus, the temporal resolution for covering multiple directions is limited. In recent years, the advanced modular incoherent scatter radar (AMISR) [*Heinselman and Nicolls*, 2008] utilizes phased array technique and enables high-resolution and multidirectional observations of the ionosphere, which are

particularly useful for studying the ionosphere response to transient solar wind perturbations, such as dynamic pressure increase.

In this study, we present a detailed case study of the ionospheric response to the solar wind dynamic pressure enhancement associated with the 17 March 2015 geomagnetic storm sudden commencement (SSC), and the resulting FACs and ionospheric convection flows by using data from Poker Flat incoherent scatter radar (PFISR) and ground-based magnetometers. We have also carried out a global MHD simulation of the coupled magnetosphere-ionosphere for this storm event to obtain a global context for interpreting localized ISR observations. Results from the global MHD simulation and their comparisons with ground-based measurements will be presented.

## 2. Observations and Modeling

### 2.1. Solar Wind and IMF Observations

The 17 March 2015 storm with the minimum *SYM-H* reaching  $-234$  nT was caused by an interplanetary coronal mass ejection (ICME) and has received much attention. The SSC at  $\sim 0445$  UT on 17 March 2015 was initiated by the shock formed in front of the ICME. Figure 1 shows the solar wind and IMF conditions propagated to the bow shock from the OMNI database. The solar wind velocity elevated from  $\sim 400$  to  $\sim 500$  km/s, while the solar wind proton number density increased from  $\sim 10$  to  $\sim 35$   $\text{cm}^{-3}$ . As a result, the dynamic pressure jumped from  $\sim 5$  to  $\sim 18$  nPa. The IMF  $B_z$  turned farther northward from  $\sim 10$  nT to  $\sim 25$  nT and lasted for more than an hour before rotated into a southward direction. In this study, we focus on the response of the ionosphere to this solar wind dynamic pressure enhancement. The bottom panel of Figure 1 shows the 1 min *SYM-H* index, from which the compressional effect of the SSC can be seen clearly at  $\sim 0445$  UT.

### 2.2. Magnetometer and PFISR Observations

Figure 2a shows the 1 s *H* component perturbation measured by the Poker Flat ground-based magnetometer from 0430 UT to 0530 UT on 17 March 2015. The perturbation shown in this panel is obtained by subtracting a baseline value, which is taken as the mean value between 0430 and 0440 UT. The perturbation shows a clear negative perturbation, i.e., the preliminary impulse (PI), at  $\sim 0445$  UT followed by a positive perturbation, i.e., the main impulse (MI), which lasted much longer. This magnetic perturbation is consistent with the classic magnetic signatures of SC.

PFISR was running in the four-beam international polar year mode before 0500 UT on 17 March 2015. There was one beam pointing in the direction parallel to the magnetic field (beam 2, UpB), one beam pointing vertically (beam 1), and two other beams pointing to higher latitudes with lower elevation angles (beams 3 and 4). At the time of the storm SSC, PFISR was located at  $\sim 17.7$  magnetic local time (MLT) on the duskside and its observations from 0430 to 0500 UT are shown in Figures 2b–2d. Figures 2b–2d show the convection flow direction, magnitude, and vector as a function of UT and magnetic latitude (MLAT), respectively. Calculations of the  $E \times B$  convection flow and the antiparallel flow from AMISR data can be found in Heinselman and Nicolls [2008]. In the Northern Hemisphere, the antiparallel direction is positive pointing to higher altitudes along the magnetic field. Given an  $\sim 78^\circ$  magnetic field inclination at PFISR, both the  $E \times B$  convection flow and the antiparallel flow can provide finite vertical flows, either positive or negative, when projected to the geographic vertical direction [Zou *et al.*, 2013, 2014]. A schematic illustration of the flow geometry is provided on the right of Figure 2f. Figure 2e shows the total plasma vertical flows calculated by combining the contributions from the  $E \times B$  convection flow and the antiparallel flow in the vertical direction. The latitudinally averaged vertical flows contributed by the  $E \times B$  convection flow (red) and the antiparallel flow (blue) are illustrated in Figure 2f. Figure 2 shows the altitude profiles of electron density measured by the vertical beam, i.e., beam 1. As one can see, in general, before the SSC, the convection flows at PFISR were very weak and the *F* region ionosphere resembled the quiet time conditions. After the SSC, there were large convection flow perturbations, *F* region plasma lifting to higher altitudes and subsequent decrease of the *F* region plasma density. As shown in Figures 2e and 2f, strong plasma vertical flows lasted about 4 min starting at the transition time from the PI to the MI phase at  $\sim 0447$  UT, and the flow speed reached  $>200$  m/s almost purely due to the contribution from the  $E \times B$  convection flows. Such vertical drift and lifting of the *F* region ionosphere have been frequently observed within the SED [Zou *et al.*, 2013, 2014] although the convection flows are associated with different magnetospheric dynamic processes. These vertical drifts and *F*

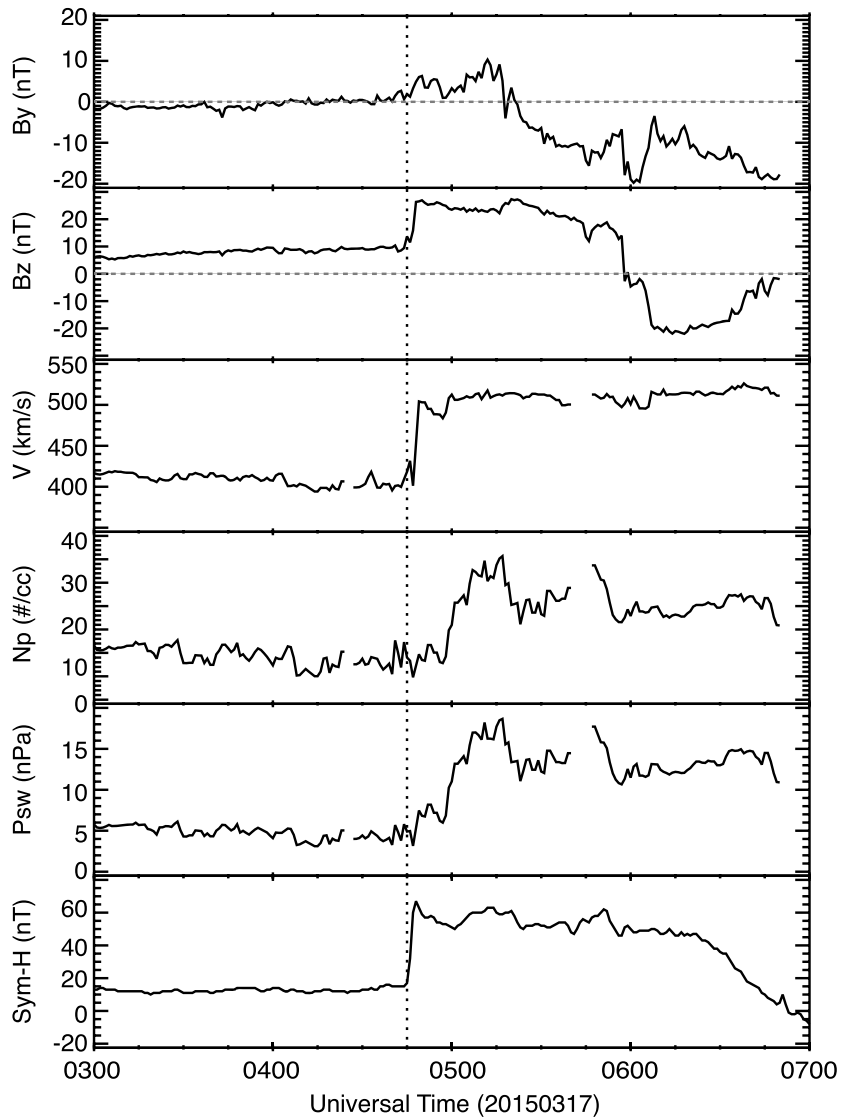


**Figure 1.** From top to bottom, IMF  $B_y$  and  $B_z$  components in the GSM coordinates, solar wind speed, proton number density, solar wind dynamic pressure, and the SYM-H index are shown for 03–07 UT on 17 March 2015. The vertical dashed line indicates the beginning of the storm sudden commencement (SSC) signature in the SYM-H index at ~0445 UT.

region lifting have been suggested to play an important role in preconditioning intense ion upflow fluxes [Zou *et al.*, 2017].

Figure 3 shows the altitude profiles of (a) electron density  $N_{er}$ , (b) line-of-sight velocity  $V_{losr}$ , (c) ion temperature  $T_{ir}$ , and (d) electron temperature  $T_e$  from the 5 min integrated long pulse measurement of the vertical beam. The 5 min integrated long pulse data are chosen to show because they have better signal-to-noise ratio (SNR) and thus are less noisy, while the 1 min integrated long pulse data have also been studied. Grey curves show the measurements obtained during the three integration time (~15 min) prior to the SSC, while colored curves show the values during the SSC and afterward. The integration time corresponding to each color curve is also denoted. The density profiles in Figure 3a indicate that the height of the F region peak density ( $h_m F_2$ ) rose from ~290 km to ~330 km, resulting in a 40 km increase. At the same time, the peak density ( $N_m F_2$ ) decreased from  $\sim 7 \times 10^{11}$  to  $4.5 \times 10^{11} \text{ m}^{-3}$ , a 36% decrease. The total electron content (TEC) calculated by integrating the density along the altitude up to the topside ionosphere (~650 km) shows a  $> 7$  TECU (1 TECU unit =  $10^{16} \text{ el/m}^2$ ) reduction when comparing the averaged TEC between 0435 and 0440 UT, i.e., 5–10 min before the compression and that between 0455 and 0500 UT, i.e., 10–15 min after the compression.

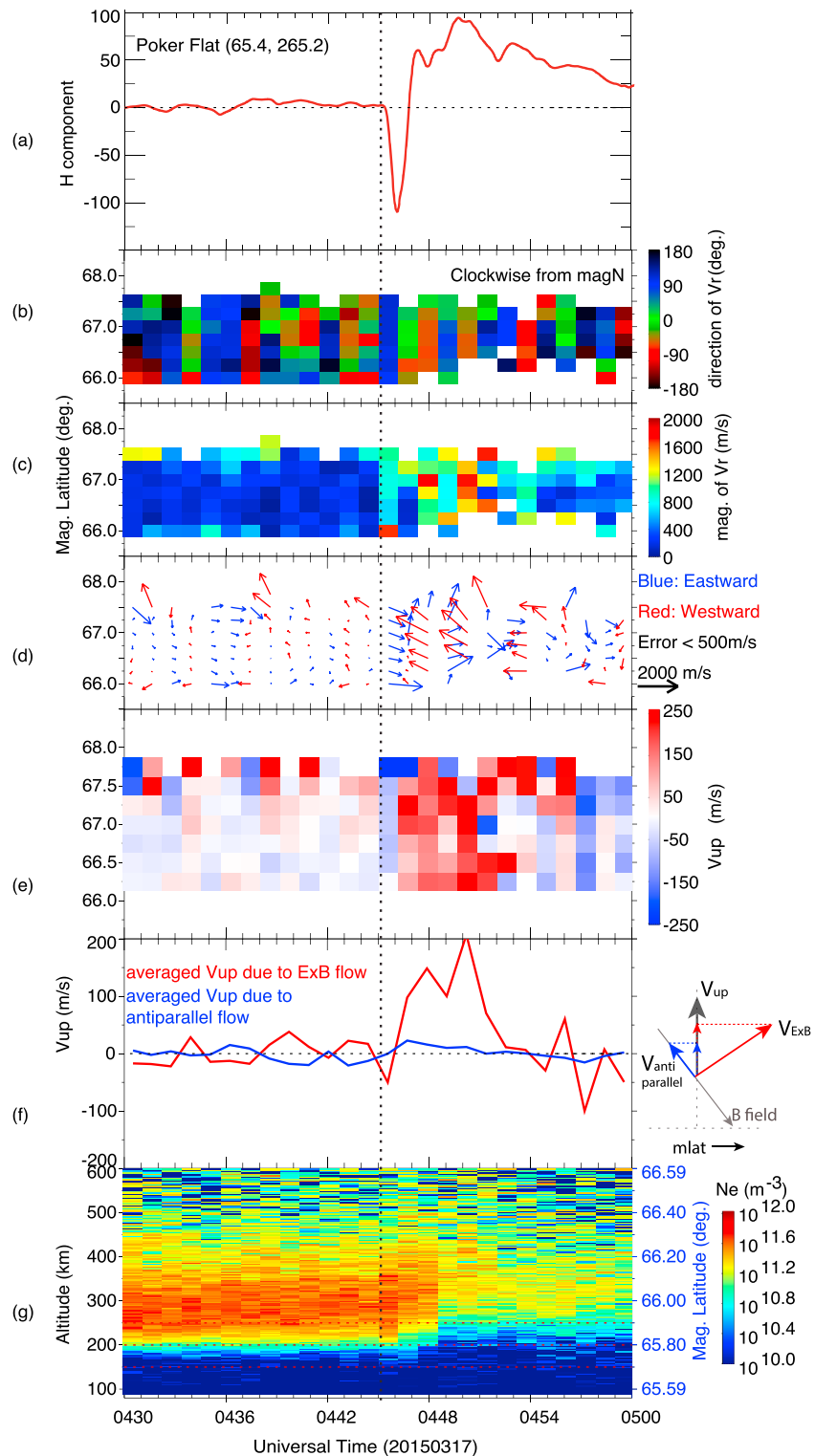


**Figure 2.** (a) The 1 s magnetic perturbation in the  $H$  component measured by the magnetometer at Poker Flat. The average value in the first 10 min has been subtracted from the measured field. The vertical dashed line indicates the beginning of the preliminary impulse (PI) phase at  $\sim 0445$  UT. PFISR measurements from 0430 to 0500 UT on 17 March 2015 are shown in Figures 2b–2g. (b)  $E \times B$  convection flow direction, (c) flow speed, (d) flow vectors, (e) calculated vertical plasma flows, (f) contribution of the vertical flows from the  $E \times B$  convection flows (red) and the antiparallel flow measured along the magnetic field line (blue), and (g) the raw electron densities with no correction for  $T_e/T_i$  or Debye length effects measured by beam 1 are shown. Beam 1 points vertically in the geographic coordinates.

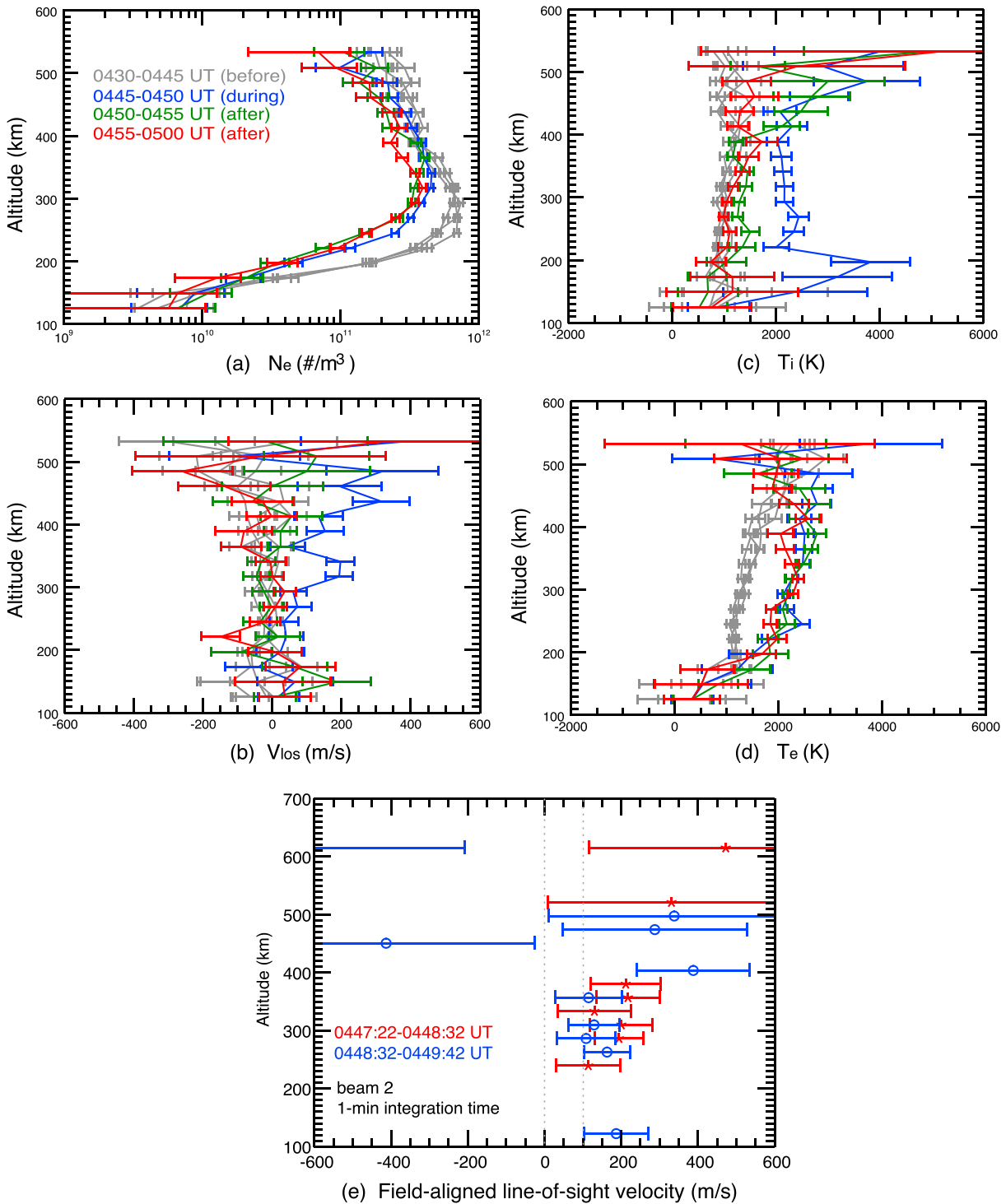


**Figure 3.** Vertical profiles of (a) electron density, (b) line-of-sight velocity, (c) ion temperature, and (d) electron temperature measured by the PFISR vertical beam 1. Grey curves show the measurements prior to the SC-related FAC passage; blue curves show the measurements during the passage of SC-related FAC; green and red curves show the measurements after the SC-related FAC. Error bars indicate the measurement uncertainties. (e) Field-aligned line-of-sight velocities measured by beam 2, i.e., the field-aligned beam, at 0447:22–0448:32 UT (red) and 0448:32–0449:42 UT (blue) are shown. Only data points with measurement uncertainty smaller than the magnitude of measurement itself are plotted. Field-aligned ion upflow event can be identified at both time cadences.



Figure 3b shows that the vertical flow velocity was, in general, around zero despite large measurement uncertainties, but the flow velocity above 250 km altitude was clearly upward immediately after the SSC, consistent with the lifting signatures in Figures 2e and 2f and the electron density in Figure 2g. In Figure 3c,  $T_i$  increased from  $\sim 1000$  K to more than 2000 K at all altitudes above  $\sim 150$  km immediately after the SSC (blue curve) but dropped back to quiet time values in the subsequent measurements  $\sim 5$  min later (green and red curves). The  $T_i$  increase was particularly large below  $\sim 200$  km albeit with relatively large uncertainties because of the low electron density in this region. In contrast,  $T_e$  shown in Figure 3d increased from below 1500 K to above 2000 K above 200 km and lasted for at least three integration time ( $\sim 15$  min) until  $\sim 0500$  UT, i.e., the end of this experiment.

A field-aligned ion upflow/downflow event is defined when three consecutive field-aligned velocity data are larger/smaller than  $100/-100$  m/s [Ogawa *et al.*, 2009]. According to this criterion, we did not find any field-aligned ion upflow events in the UpB beam (beam 2) in the 5 min integrated long pulse data. We, therefore, turned to the 1 min integrated long pulse data of the UpB beam to examine whether there are signatures of field-aligned ion upflow. Figure 3e shows the 1 min field-aligned line-of-sight velocity measured by beam 2 from 0447:22 UT to 0449:42 UT (i.e.,  $\sim 2$  min interval). Because of short integration time, the data become very noisy. Only data points with measurement uncertainties smaller than the magnitude of measurement itself are plotted here. Two dashed vertical lines at 0 m/s and 100 m/s are plotted to help identify the upflow event. The averaged field-aligned ion upflow velocity from range gate 7 to range gate 11 (i.e., from 274 km to 392 km) during 0447:22–0448:32 UT (red) reached  $\sim 190.7$  m/s, while that from range gate 6 to range gate 8 (i.e., from 250 km to 321 km) at 0448:32–0449:42 UT (blue) reached  $\sim 133.5$  m/s. Collis and Häggström [1991] commented that they did not find field-aligned ion upflow during the SC event they studied. To the best of our knowledge, this transient field-aligned ion upflow due to SC have not been reported before.

The  $T_i$  increase occurred at the same time as the SC-related convection flow speed increase, and therefore, this increase is likely due to enhanced frictional heating. Similar but persistent  $T_i$  and  $V_{\text{los}}$  increases due to frictional heating have also been observed during the main phase of the same storm but in the subauroral polarization stream (SAPS) region by the Millstone Hill radar [Zhang *et al.*, 2017]. Significant and persistent frictional heating can also increase the neutral temperature and lead to neutral upwelling, as found in the SAPS region by Zhang *et al.* [2017]. However, because the neutrals need much longer time (tens of minutes to days) to respond to frictional heating [Schunk and Nagy, 2009], it is unlikely to have such neutral upwelling formed within the first 5–10 min right after the onset of the strong horizontal flows due to the SC.

The cause of the long-lasting  $T_e$  increase appears more complicated and could be due to a combined effect of electron density reduction and potential particle precipitations associated with upward FACs related to the SC. Assuming no extra incoming energy, the electron temperature and the density should be anticorrelated with each other [Schunk and Nagy, 2009]. So if the electron density decreases, its temperature can increase. The observed plasma temperature changes and their temporal variations are consistent with the simulation results reported in Schunk *et al.* [1994], who showed short-lived  $T_i$  enhancement at the front of vortices and long-lasting  $T_e$  effect in the wake of vortices.

The blue curve in Figure 3c shows that  $T_i$  was larger than  $T_e$  and there was a temperature bulge in the  $T_i$  profile near  $\sim 200$  km. This could be a signature of enhanced frictional heating, but the retrieval of  $T_i$  in ISR fitting is also subject to uncertainties with the assumption of stationarity and with the assumed molecular ions concentrations [Zettergren *et al.*, 2011]. Rapidly varying line-of-sight velocities over the integration period can broaden the integrated spectrum, leading to an overestimation of ion temperature after fitting, but in this case this effect is not expected to be significant because the high temperatures are still observed when the data are reprocessed with a 1 min integration time. Intense frictional heating events will also increase the fractional concentration of  $\text{NO}^+$  since the  $\text{O}^+ + \text{N}_2 \rightarrow \text{NO}^+ + \text{N}$  reaction is highly temperature dependent [Schunk and Nagy, 2009]. The standard PFISR data fitting procedure uses the FLIP chemistry model developed by Richards and Voglozin [2011], so the effect of the chemical composition change has been considered here to within the limits of validity of that model. After the convection flow enhancements and plasma temperature increases, the concentrations of molecular ions  $\text{NO}^+$  and  $\text{O}_2^+$  increased to  $\sim 84\%$  and  $\sim 12\%$  at the range gate of 197 km, respectively, and the  $\text{O}^+$  concentration decreased to  $\sim 3\%$ . In addition, we have also explored the sensitivity of the estimated  $T_i$  by investigating an ensemble of composition profiles and assuming the original fitter correctly estimated the density weighted average  $T_i/m_i$  (see supporting

information  $S_1$ ). While the  $T_i$  temperature bulge becomes less prominent when the transition height is lower, it still exists even with the lowest transition height tested. This experiment suggests that the temperature bulge in the  $T_i$  altitude profile observed near 200 km is likely due to very strong frictional heating and not purely due to the ion composition changes.

As shown in Schunk *et al.* [1994], the perpendicular ion temperature is expected to be much higher than the parallel temperature. PFISR observations show less  $T_i$  enhancement in the UpB beam and more  $T_i$  enhancement in the two lower elevation beams, as expected if  $T_{\text{perp}} > T_{\text{parallel}}$ . However, we have attempted to derive the temperature anisotropy by using different combinations of the four beams and assuming spatial uniformity, and our analysis yielded different results, implying that the temperature enhancements are not spatially uniform between the beams. Accurate determination of the temperature anisotropy would require improved measurement techniques, such as multiple ISRs [e.g., Ogawa *et al.*, 2000] or bistatic measurements. In addition, non-Maxwellian ion distribution functions in the perpendicular plane can lead to systematic overestimation of ion temperature when observed at large aspect angles and underestimation of ion temperature when observed at small aspect angles [Winsor *et al.*, 1989]. None of the ISR spectra in any of the beams show the formation of a central peak associated with non-Maxwellian ion distribution functions; however, all of the beams in this experiment have small aspect angles ( $<15^\circ$ ) and are not expected to be sensitive to non-Maxwellian distribution function signatures. The properties of the perpendicular ion distribution function cannot be determined from the beam geometry in this experiment.

### 2.3. Global MHD Simulation

To investigate the ground magnetic field perturbations associated with the TCVs due to solar wind pressure enhancement, their propagation and the associated currents, we have performed a global MHD simulation by using the coupled Block-Adaptive Tree Solarwind Roe-type Upwind Scheme (BATS-R-US) [Tóth *et al.*, 2012], Ridley ionosphere electrodynamic module [Ridley *et al.*, 2004], and comprehensive ring current model (CRCM) [Fok *et al.*, 2001; Buzulukova *et al.*, 2010; Glocer *et al.*, 2013]. Solar wind and IMF observations from the Wind spacecraft have been used as upstream conditions to drive the coupled model. Because of the uncertainty of solar wind and IMF propagation from the spacecraft to the upstream boundary of the simulation, the modeled results have been shifted 16 min to match the observed compression time registered in the *SYM-H* index.

A virtual ground magnetometer [Yu and Ridley, 2011] at the location of Poker Flat has been included in the simulation. The simulated  $H$  component perturbations at Poker Flat are shown in Figure 4a (blue), which agrees very well with the observation at Poker Flat (red). The good agreement between the observed and modeled magnetic perturbations provides us confidence in using the global model to study the pressure-induced FACs, convection and their evolution, and to interpret the PFISR observations presented above.

Besides the virtual magnetometer at Poker Flat, a total of 100 uniformly distributed virtual magnetometers between  $50^\circ$  and  $80^\circ$  MLAT and every 2 h of MLT in the Northern Hemisphere have also been included in the simulation and their  $H$  component perturbations are shown as color contours in Figures 4b and 4c at the time of the dip of the PI phase and the peak of the MI phases. The location of Poker Flat is denoted by the cyan dots. Contributions to the  $H$  component perturbation from four different types of currents, including Hall and Pederson currents, FACs, and magnetospheric currents, have been quantified and compared (not shown). We found that the dominant contribution to the total perturbation is the Hall currents, consistent with the *Fukushima* theory [Fukushima, 1976].

At 0446 UT, the negative PI phase observed at Poker Flat was part of a cloud of negative perturbation surrounding the dayside (Figure 4b). The FACs superimposed with convection contours on top are shown in Figures 5d and 5e. The FACs plot in Figure 4d shows that around this time, Poker Flat was located close to the boundary between the downward FACs associated with the PI and the upward FACs associated with the MI. Thus, the negative perturbation can be understood to be due to the Hall currents flowing northward between the two FAC systems.

The FACs continue to propagate with time from the dayside to the nightside as well as moving poleward. Consequently, the positive  $H$  perturbation observed by the Poker Flat magnetometer around 0448 UT during the MI phase was part of the positive perturbation cloud (Figure 4c) and was due to the Hall currents flowing southeastward between the MI upward FACs and the weak downward FACs at lower latitudes.



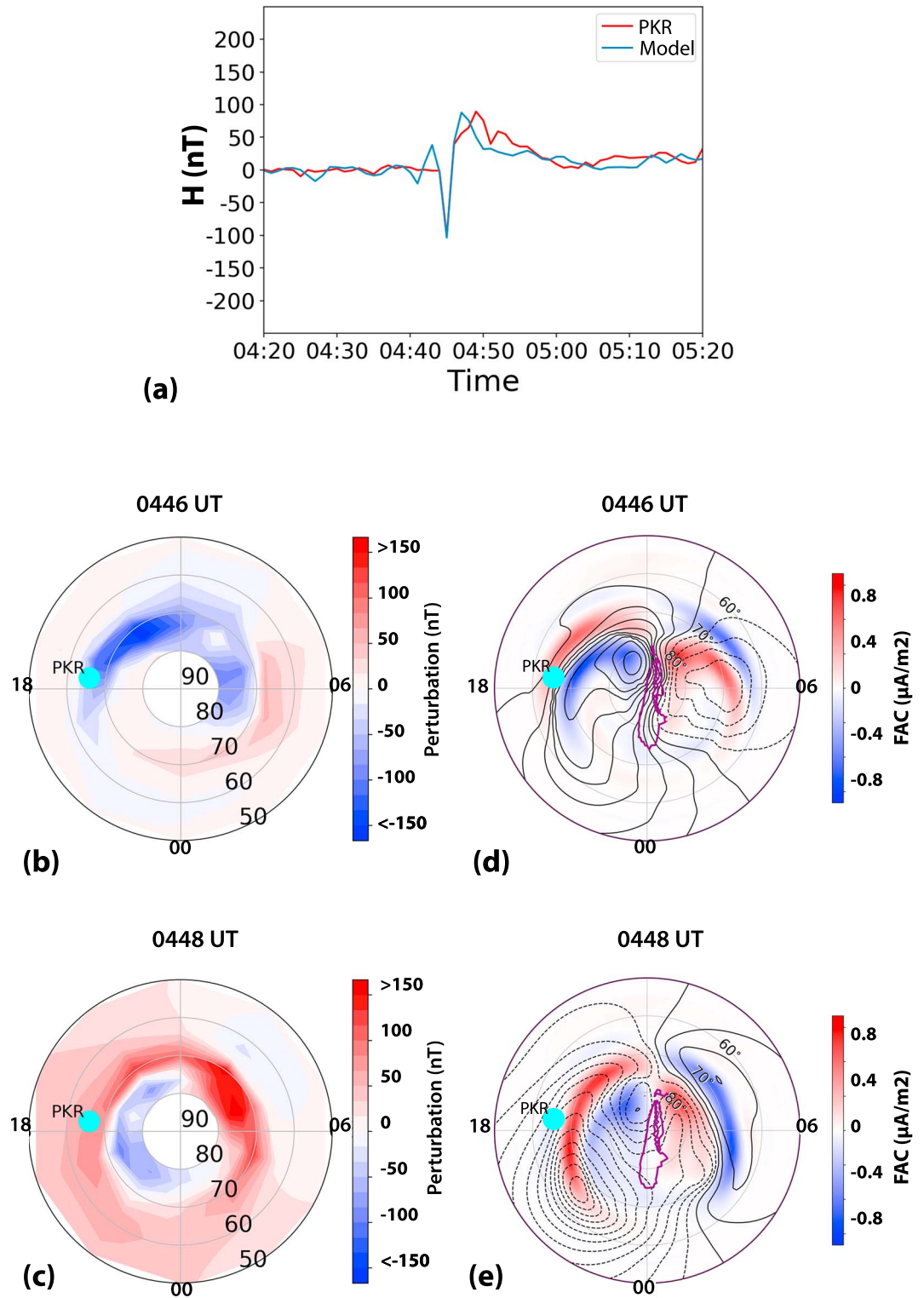


**Figure 4.** (a) Comparison between the simulated magnetic perturbations in the  $H$  component and the observations at Poker Flat. One minute time resolution data are used here. (b–c) Two-dimensional distribution of simulated magnetic perturbations in the  $H$  component at the dip of the PI phase and the peak of the MI phase in the Northern Hemisphere. (d, e) Two-dimensional distribution of simulated field-aligned currents (FACs) and convection equipotentials in the Northern Hemisphere. The open-closed field line boundary is shown as purple lines.

The polarities of FACs can also be inferred from the convection flow measurements from PFISR in Figure 2. The results are consistent with the findings from our global simulation. That is, the closure Hall currents poleward and equatorward of the upward FACs passed PFISR during the PI and MI phases sequentially. The  $F$  region lifting observed in Figure 2 happened mainly due to the poleward and northwestward convection flows during the transition from the PI phase to the MI phase.

### 3. Summary and Conclusions

SCs due to the solar wind dynamic pressure enhancements have been studied extensively using ground magnetometers and SuperDARN radars, while only very limited studies have been reported about the effects of the SC on the ionospheric plasma. Here we report detailed PFISR observations of the ionospheric responses to the solar wind dynamic pressure enhancement during the SSC of the 17 March 2015 storm. The ground magnetometer at Poker Flat was used to identify the PI and MI phases. During the transition from the PI phase to the MI phase, PFISR observed lifting of the  $F$  region ionosphere, large and transient field-aligned ion upflow, prompt but short-lived ion temperature increase. During the MI phase, PFISR observed  $F$  region density decrease and persistent electron temperature increase in the wake region of the ionospheric flow vortices. The TEC calculated from PFISR density measurement shows a  $> 7$  TECU decrease within a couple of minutes. A global BATS-R-US MHD simulation has been conducted for this event to put localized PFISR observations into a global context. The simulation reveals the distribution of large-scale FACs during the PI and MI phases and their evolution and propagation through the polar cap. The simulated  $H$  component magnetic perturbations at virtual magnetometers placed in the simulation show satisfactory agreement with the Poker Flat magnetometer observations. Based on the simulation results, we demonstrate that the characteristic variations of the ionospheric plasma observed by PFISR are indeed produced by the passage of SC-related current systems.

Combining the observations and numerical simulations together, this case study suggests that transient field-aligned ion upflow and  $F$  region ionosphere lifting due to large vertical flows can be generated due to the SC-related FACs and ionospheric convection flows, providing a plausible explanation for why ion upflow and outflow fluxes increase after the solar wind dynamic pressure increases. Such ionospheric plasma responses should be expected to occur in regions to which the SC-related FACs propagate and thus may have a global impact, which will be a target of future research. In addition, these observations, for the first time, provide a comprehensive observational confirmation of previous ionospheric simulations on the effects of propagating ionospheric vortices and FAC pairs. Moreover, a deeper understanding of the ionospheric plasma response to SC and the related FAC system and convection changes will advance our capabilities of forecasting the ionosphere TEC and coherent radar coverage.

#### Acknowledgments

We thank the two anonymous reviewers for their very constructive comments. The research at University of Michigan is supported by NSF AGS 1342968 and NASA NNX14AF31G. We acknowledge use of NASA/GSFC's Space Physics Data Facility's OMNIWeb (or CDAWeb, <https://cdaweb.sci.gsfc.nasa.gov/index.html/>) service, and the OMNI data and  $SYM-H$  index. The 1 s Poker Flat magnetometer data were obtained from the Geophysical Institute, UAF 2016 (<https://www.asf.alaska.edu/magnetometer/download/>), and the 1 min Poker Flat magnetometer data were obtained from the SuperMag website (<http://supermag.jhuapl.edu/>). SWMF simulations are performed using the NSF Yellowstone supercomputing facility and will be available by request (shashaz@umich.edu).

#### References

- Araki, T. (1977), Global structure of geomagnetic sudden commencements, *Planet. Space Sci.*, *25*(4), 373–384, doi:10.1016/0032-0633(77)90053-8.
- Araki, T. (1994) A physical model of the geomagnetic sudden commencement, in *Solar Wind Sources of Magnetospheric Ultra-Low-Frequency Waves*, edited by M. J. Engebretson, K. Takahashi and M. Scholer, pp. 183–200, AGU, Washington, D. C., doi:10.1029/GM081p0183.
- Buzulukova, N., M.-C. Fok, J. Goldstein, P. Valek, D. J. McComas, and P. C. Brandt (2010), Ring current dynamics in moderate and strong storms: Comparative analysis of TWINS and IMAGE/HENA data with the Comprehensive Ring Current Model: STRONG STORM VERSUS MODERATE STORM, *J. Geophys. Res.*, *115*, A12234, doi:10.1029/2010JA015292.
- Chappell, C. R. (2015), The role of the ionosphere in providing plasma to the terrestrial magnetosphere—An historical overview, *Space Sci. Rev.*, *192*(1–4), 5–25, doi:10.1007/s11214-015-0168-5.
- Chi, P. J., D.-H. Lee, and Russell C. T. (2006), Tamao travel time of sudden impulses and its relationship to ionospheric convection vortices, *J. Geophys. Res.*, *111*, A08205, doi:10.1029/2005JA011578.
- Collis, P. N., and I. Häggström (1991), High-latitude ionospheric response to a geomagnetic sudden commencement, *J. Atmos. Terr. Phys.*, *53*(3–4), 241–248, doi:10.1016/0021-9169(91)90108-J.
- Curto, J. J., T. Araki, and L. F. Alberca (2007), Evolution of the concept of sudden storm commencements and their operative identification, *Earth, Planets Space*, *59*(11), i–xii, doi:10.1186/BF03352059.
- Doupnik, J. R., A. Brekke, and P. M. Banks (1977), Incoherent scatter radar observations during three sudden commencements and a Pc 5 event on August 4, 1972, *J. Geophys. Res.*, *82*, 499–514, doi:10.1029/JA082i004p00499.
- Fok, M.-C., R. A. Wolf, R. W. Spiro, and T. E. Moore (2001), Comprehensive computational model of Earth's ring current, *J. Geophys. Res.*, *106*, 8417–8424, doi:10.1029/2000JA000235.
- Foster, J. C., et al. (2005), Multiradar observations of the polar tongue of ionization, *J. Geophys. Res.*, *110*, A09S31, doi:10.1029/2004JA010928.
- Friis-Christensen, E., M. A. McHenry, C. R. Clauer, and S. Vennerström (1988), Ionospheric traveling convection vortices observed near the polar cleft: A triggered response to sudden changes in the solar wind, *Geophys. Res. Lett.*, *15*, 253–256, doi:10.1029/GL015i003p00253.

- Fujita, S., T. Tanaka, T. Kikuchi, K. Fujimoto, K. Hosokawa, and M. Itonaga (2003a), A numerical simulation of the geomagnetic sudden commencement: 1. Generation of the field-aligned current associated with the preliminary impulse, *J. Geophys. Res.*, *108*(A12), 1416, doi:10.1029/2002JA009407.
- Fujita, S., T. Tanaka, T. Kikuchi, K. Fujimoto, and M. Itonaga (2003b), A numerical simulation of the geomagnetic sudden commencement: 2. Plasma processes in the main impulse, *J. Geophys. Res.*, *108*(A12), 1417, doi:10.1029/2002JA009763.
- Fujita, S., T. Tanaka, and T. Motoba (2005), A numerical simulation of the geomagnetic sudden commencement: 3. A sudden commencement in the magnetosphere-ionosphere compound system, *J. Geophys. Res.*, *110*, A11203, doi:10.1029/2005JA011055.
- Fukushima, N. (1976), Generalized theorem for no ground magnetic effect of vertical currents connected with Pedersen currents in the uniform-conductivity ionosphere, *Rep. Ionos. Space Res. Jpn.*, *30*, 1–2.
- Gillies, D. M., J.-P. St.-Maurice, K. A. McWilliams, and S. Milan (2012), Global-scale observations of ionospheric convection variation in response to sudden increases in the solar wind dynamic pressure, *J. Geophys. Res.*, *117*, A04209, doi:10.1029/2011JA017255.
- Glassmeier, K.-H., M. Hönisch, and J. Untiedt (1989), Ground-based and satellite observations of traveling magnetospheric convection twin vortices, *J. Geophys. Res.*, *94*, 2520, doi:10.1029/JA094iA03p02520.
- Glocer, A., M. Fok, X. Meng, G. Toth, N. Buzulukova, S. Chen, and K. Lin (2013), CRCM + BATS-R-US two-way coupling, *J. Geophys. Res. Space Physics*, *118*, 1635–1650, doi:10.1002/jgra.50221.
- Heinselman, C. J., and M. J. Nicolls (2008), A Bayesian approach to electric field and *E* region neutral wind estimation with the Poker Flat Advanced Modular Incoherent Scatter Radar, *Radio Sci.*, *43*, RS5013, doi:10.1029/2007RS003805.
- Kane, T. A., and R. A. Makarevich (2010), HF radar observations of the *F* region ionospheric plasma response to Storm Sudden Commencements, *J. Geophys. Res.*, *115*, A07320, doi:10.1029/2009JA014974.
- Kataoka, R., H. Fukunishi, K. Hosokawa, H. Fujiwara, A. S. Yukimatu, N. Sato, and Y.-K. Tung (2003), Transient production of *F* region irregularities associated with TCV passage, *Ann. Geophys.*, *21*(7), 1531–1541, doi:10.5194/angeo-21-1531-2003.
- Kikuchi, T., S. Tsunomura, K. Hashimoto, and K. Nozaki (2001), Field-aligned current effects on midlatitude geomagnetic sudden commencements, *J. Geophys. Res.*, *106*, 15555–15565, doi:10.1029/2001JA900030.
- Kivelson, M. G., and D. J. Southwood (1991), Ionospheric traveling vortex generation by solar wind buffeting of the magnetosphere, *J. Geophys. Res.*, *96*, 1661–1667, doi:10.1029/90JA01805.
- Kubota, Y., R. Kataoka, M. Den, T. Tanaka, T. Nagatsuma, and S. Fujita (2015), Global MHD simulation of magnetospheric response of preliminary impulse to large and sudden enhancement of the solar wind dynamic pressure, *Earth, Planets Space*, *67*(1), doi:10.1186/s40623-015-0270-7.
- Lanzerotti, L. J., R. M. Konik, A. Wolfe, D. Venkatesan, and C. G. MacLennan (1991), Cusp latitude magnetic impulse events: 1. Occurrence statistics, *J. Geophys. Res.*, *96*, 14009–14022, doi:10.1029/91JA00567.
- Liu, H., and G. Lu (2004), Velocity shear-related ion upflow in the low-altitude ionosphere, *Ann. Geophys.*, *22*, 1149–1153, doi:10.5194/angeo-22-1149-2004.
- Lotko, W. (2007), The magnetosphere–ionosphere system from the perspective of plasma circulation: A tutorial, *J. Atmos. Sol.-Terr. Phys.*, *69*(3), 191–211, doi:10.1016/j.jastp.2006.08.011.
- Lühr, H., W. Blawert, and H. Todd (1993), The ionospheric plasma flow and current patterns of travelling convection vortices: A case study, *J. Atmos. Terr. Phys.*, *55*(14), 1717–1727, doi:10.1016/0021-9169(93)90140-T.
- Moen, J., K. Oksavik, and H. C. Carlson (2004), On the relationship between ion upflow events and cusp auroral transients, *Geophys. Res. Lett.*, *31*, L11808, doi:10.1029/2004GL020129.
- Moretto, T., E. Friis-Christensen, H. Lühr, and E. Zesta (1997), Global perspective of ionospheric traveling convection vortices: Case studies of two Geospace Environmental Modeling events, *J. Geophys. Res.*, *102*, 11597–11610, doi:10.1029/97JA00324.
- Murr, D. L., W. J. Hughes, A. S. Rodger, E. Zesta, H. U. Frey, and A. T. Weatherwax (2002), Conjugate observations of traveling convection vortices: The field-aligned current system, *J. Geophys. Res.*, *107*(A10), 1306, doi:10.1029/2002JA009456.
- Murr, D. L., and W. J. Hughes (2003), Solar wind drivers of Traveling Convection Vortices, *Geophys. Res. Lett.*, *30*(7), 1354, doi:10.1029/2002GL015498.
- Nilsson, H., et al. (2008), Transients in oxygen outflow above the polar cap as observed by the Cluster spacecraft, *Ann. Geophys.*, *26*(11), 3365–3373, doi:10.5194/angeo-26-3365-2008.
- Nishida, A., and J. A. Jacobs (1962), World-wide changes in the geomagnetic field, *J. Geophys. Res.*, *67*, 525–540, doi:10.1029/JZ067i002p00525.
- Ogawa, Y., S. C. Buchert, R. Fujii, S. Nozawa, and A. P. van Eyken (2009), Characteristics of ion upflow and downflow observed with the European Incoherent Scatter Svalbard radar, *J. Geophys. Res.*, *114*, A05305, doi:10.1029/2008JA013817.
- Ogawa, Y., R. Fujii, S. C. Buchert, S. Nozawa, S. Watanabe, and A. P. van Eyken (2000), Simultaneous EISCAT Svalbard and VHF radar observations of ion upflows at different aspect angles, *Geophys. Res. Lett.*, *27*, 81–84, doi:10.1029/1999GL010665.
- Richards, P. G., and D. Voglozin (2011), Reexamination of ionospheric photochemistry, *J. Geophys. Res.*, *116*, A08307, doi:10.1029/2011JA016613.
- Ridley, A. J., T. I. Gombosi, and D. L. DeZeeuw (2004), Ionospheric control of the magnetosphere: Conductance, *Ann. Geophys.*, *22*(2), 567–584, doi:10.5194/angeo-22-567-2004.
- Samsonov, A. A., D. G. Sibeck, and Y. Yu (2010), Transient changes in magnetospheric-ionospheric currents caused by the passage of an interplanetary shock: Northward interplanetary magnetic field case, *J. Geophys. Res.*, *115*, A05207, doi:10.1029/2009JA014751.
- Schunk, R., and A. Nagy (2009) *Ionospheres: Physics, Plasma Physics, and Chemistry*, pp. 231–252, Cambridge Univ. Press, Cambridge.
- Schunk, R. W., L. Zhu, and J. J. Sojka (1994), Ionospheric response to traveling convection twin vortices, *Geophys. Res. Lett.*, *21*, 1759–1762, doi:10.1029/94GL01059.
- Semeter, J., C. J. Heinselman, J. P. Thayer, R. A. Doe, and H. U. Frey (2003), Ion upflow enhanced by drifting *F* region plasma structure along the nightside polar cap boundary, *Geophys. Res. Lett.*, *30*(22), 2139, doi:10.1029/2003GL017747.
- Shi, Q. Q., et al. (2014), Solar wind pressure pulse-driven magnetospheric vortices and their global consequences, *J. Geophys. Res. Space Physics*, *119*, 4274–4280, doi:10.1002/2013JA019551.
- Sibeck, D. G., and G. I. Korotova (1996), Occurrence patterns for transient magnetic field signatures at high latitudes, *J. Geophys. Res.*, *101*, 13413–13428, doi:10.1029/96JA00187.
- Sibeck, D. G., N. B. Trivedi, E. Zesta, R. B. Decker, H. J. Singer, A. Szabo, H. Tachihara, and J. Watermann (2003), Pressure-pulse interaction with the magnetosphere and ionosphere, *J. Geophys. Res.*, *108*(A2), 1095, doi:10.1029/2002JA009675.
- Slinker, S. P., J. A. Fedder, W. J. Hughes, and J. G. Lyon (1999), Response of the ionosphere to a density pulse in the solar wind: Simulation of traveling convection vortices, *Geophys. Res. Lett.*, *26*, 3549–3552, doi:10.1029/1999GL010688.
- Strangeway, R. J., R. E. Ergun, Y.-J. Su, C. W. Carlson, and R. C. Elphic (2005), Factors controlling ionospheric outflows as observed at intermediate altitudes, *J. Geophys. Res.*, *110*, A03221, doi:10.1029/2004JA010829.

- Sun, T. R., C. Wang, J. J. Zhang, V. A. Pilipenko, Y. Wang, and J. Y. Wang (2015), The chain response of the magnetospheric and ground magnetic field to interplanetary shocks, *J. Geophys. Res. Space Physics*, *120*, 157–165, doi:10.1002/2014JA020754.
- Tian, A. M., X. C. Shen, Q. Q. Shi, B. B. Tang, M. Nowada, Q. G. Zong, and S. Y. Fu (2016), Dayside magnetospheric and ionospheric responses to solar wind pressure increase: Multispacecraft and ground observations, *J. Geophys. Res. Space Physics*, *121*, 10,813–10,830, doi:10.1002/2016JA022459.
- Tóth, G. et al. (2012), Adaptive numerical algorithms in space weather modeling, *J. Comput. Phys.*, *231*(3), 870–903, doi:10.1016/j.jcp.2011.02.006.
- Winsor, K. J., M. Lockwood, G. O. L. Jones, and K. Suvanto (1989), Observations of nonthermal plasmas at different aspect angles, *J. Geophys. Res.*, *94*, 1439–1449, doi:10.1029/JA094iA02p01439.
- Yau, A. W., T. Abe, and W. K. Peterson (2007), The polar wind: Recent observations, *J. Atmos. Sol. Terr. Phys.*, *69*(16), 1936–1983, doi:10.1016/j.jastp.2007.08.010.
- Yu, Y.-Q., and A. J. Ridley (2011), Understanding the response of the ionosphere-magnetosphere system to sudden solar wind density increases, *J. Geophys. Res.*, *116*, A04210, doi:10.1029/2010JA015871.
- Yuan, Z.-G., X.-H. Deng, and J.-F. Wang (2008), DMSP/GPS observations of intense ion upflow in the midnight polar ionosphere associated with the SED plume during a super geomagnetic storm, *Geophys. Res. Lett.*, *35*, L19110, doi:10.1029/2008GL035462.
- Zesta, E. (2002), A statistical study of traveling convection vortices using the Magnetometer Array for Cusp and Cleft Studies, *J. Geophys. Res.*, *107*(A10), 1317, doi:10.1029/1999JA000386.
- Zesta, E., W. J. Hughes, M. J. Engebretson, T. J. Hughes, A. J. Lazarus, and K. I. Paularena (1999), The November 9, 1993, traveling convection vortex event: A case study, *J. Geophys. Res.*, *104*, 28041–28058, doi:10.1029/1999JA900306.
- Zettergren, M., J. Semeter, C. Heinselman, and M. Diaz (2011), Incoherent scatter radar estimation of *F* region ionospheric composition during frictional heating events, *J. Geophys. Res.*, *116*, A01318, doi:10.1029/2010JA016035.
- Zhang, S.-R., P. J. Erickson, Y. Zhang, W. Wang, C. Huang, A. J. Coster, J. M. Holt, J. F. Foster, M. Sulzer, and R. Kerr (2017), Observations of ion-neutral coupling associated with strong electrodynamic disturbances during the 2015 St. Patrick's Day storm, *J. Geophys. Res. Space Physics*, *122*, 1314–1337, doi:10.1002/2016JA023307.
- Zou, S., M. B. Moldwin, M. J. Nicolls, A. J. Ridley, A. J. Coster, E. Yizengaw, L. R. Lyons, and E. F. Donovan (2013), Electrodynamics of the high-latitude trough: Its relationship with convection flows and field-aligned currents, *J. Geophys. Res. Space Physics*, *118*, 2565–2572, doi:10.1002/jgra.50120.
- Zou, S., M. B. Moldwin, A. J. Ridley, M. J. Nicolls, A. J. Coster, E. G. Thomas, and J. M. Ruohoniemi (2014), On the generation/decay of the storm-enhanced density plumes: Role of the convection flow and field-aligned ion flow, *J. Geophys. Res. Space Physics*, *119*, 8543–8559, doi:10.1002/2014JA020408.
- Zou, S., A. Ridley, X. Jia, E. Boyd, M. Nicolls, A. Coster, E. Thomas, and J. M. Ruohoniemi (2017), PFISR observation of intense ion upflow fluxes associated with an SED during the 1 June 2013 geomagnetic storm, *J. Geophys. Res. Space Physics*, *122*, 2589–2604, doi:10.1002/2016JA023697.